Journal of Alloys and Compounds 728 (2017) 112–117

Contents lists available at ScienceDirect

Journal of Alloys and Compounds

journal homepage: http://www.elsevier.com/locate/jalcom

Distribution of the microalloying element Cu in B_4C-reinforced 6061Al composites

Y.T. Zhou [a], Y.N. Zan [a], S.J. Zheng [a], Q.Z. Wang [b, *], B.L. Xiao [a], X.L. Ma [a, c, **], Z.Y. Ma [a]

[a] Shenyang National Laboratory for Materials Science, Institute of Metal Research, Chinese Academy of Sciences, 72 Wenhua Road, 110016, Shenyang, China
[b] CAS Key Laboratory of Nuclear Materials and Safety Assessment, Institute of Metal Research, Chinese Academy of Sciences, 72 Wenhua Road, Shenyang, 110016, China
[c] School of Materials Science and Engineering, Lanzhou University of Technology, 730050, Lanzhou, China

ARTICLE INFO

Article history:
Received 17 July 2017
Received in revised form
28 August 2017
Accepted 29 August 2017
Available online 1 September 2017

Keywords:
Aluminum matrix composite
Boron carbide
Electron microscopy
Microalloying
Interface

ABSTRACT

Cu is an important microalloying element in Al-Mg-Si (6xxx series) alloys, but its role in B_4C-reinforced Al-Mg-Si composites is rarely known. In this work, using the state-of-the-art Cs-corrected transmission electron microscopy (TEM), the Cu-related precipitation in a B_4C/6061 Al composite fabricated at different temperatures is revealed at an atomic level. In the composite hot-pressed at 560 °C, Q phase is the main Cu-contained precipitates. When the pressing temperature increases to 620 °C, the chemical reactions between B_4C reinforcements and the alloy matrix generate Al_3BC and MgB_2. Moreover, Cu is found to segregate at the interfaces between precipitates and the matrix, which is assumed to increase the nucleation of the reaction products.

1. Introduction

Due to the lightweight, high stiffness, and particularly the specific capacity for neutron absorption, B_4C particles-reinforced aluminum matrix composite (AMC) is of particular interest in the nuclear industry in these years [1–5]. They have been widely used as neutron absorber materials in the transport and storage of spent nuclear fuels.

In industrial application, Al-Mg-Si (6xxx series) alloys are commonly used for fabricating B_4C-reinforced AMCs [6]. In these alloys, addition of small amount of Cu, which is called microalloying [7], has been proved to increase the peak hardness and thermal stability of the materials [8–10]. Previous research demonstrated that Cu addition mainly alters the precipitation and the hardening kinetics [11,12]. Various types of Cu-contained precipitates in Al-Mg-Si-Cu alloys have been identified by microscopic investigations [13–16].

In contrast to the increasing knowledge of the microalloying effect of Cu in Al-Mg-Si alloys, when the alloys serve as the matrix of B_4C-reinforced AMCs, the effect, even the distributions of Cu in B_4C-reinforced AMCs is far from known. It should be noted that B_4C particles are very reactive with molten Al [17,18]. The interfacial reactions between the reinforcements and the matrix may severely consume the alloying elements and change the precipitation [19,20]. It is unclear whether the alloying Cu would involve in the chemical reactions and what the role it would play. The lacking information may limit our understanding of the microalloying effect of Cu in B_4C reinforced Al-Mg-Si composites.

Detection of microalloying elements in alloys has been a long-term challenge for conventional analytic instruments due to their resolution deficiency. Recently developed aberration-corrected transmission electron microscopy (TEM) provides us a large opportunity to directly visualize the elements' distributions [21,22]. In the present work, such imaging technique was applied to study the precipitates as well as the Cu redistributions in the neutron absorber B_4C/6061Al composites. The structural information is believed to be beneficial for the manufacture and further development of B_4C reinforced AMCs.

2. Experimental procedures

26 wt% B_4C reinforced 6061Al composites were fabricated by

* Corresponding author.
** Corresponding author.
E-mail addresses: qzhwang@imr.ac.cn (Q.Z. Wang), xlma@imr.ac.cn (X.L. Ma).

http://dx.doi.org/10.1016/j.jallcom.2017.08.273
0925-8388/

powder metallurgy (PM) technique. High purity aluminum (99.9 pct. purity) and B_4C (96.5 pct. purity) powders were used for PM fabrication. The impurities in B_4C powders are free B, C and some oxides containing Fe, Si and V. Most of these oxide impurities were removed by acid cleaning. After then, the B_4C particles were cleaned by water and dried at 150 °C for 8 h. The nominal composition of the Al matrix is Al–1.0Mg–0.65Si–0.25Cu (wt.%). The Al powder was then mechanically mixed with the B_4C particles in a bi-axis rotary mixer with a rotation speed of 50 rpm for 8 h to guarantee the homogeneity of the component. The as-mixed powders were cold compacted in a cylindrical die under a pressure of 20 MPa and then hot pressed under 50 MPa in a vacuum chamber for 2 h at different temperatures in order to control the chemical reactions between B_4C and Al. In this work, two typical composites hot-pressed at 560 °C and 620 °C were chosen to investigate, since partial liquid phase appears in the Al matrix above 600 °C and the interfacial reactions become obvious. To further increase the density and mechanical properties of the composites, the hot-pressed billets were forged to discs with 12 mm in thickness at 480 °C. The actual density of the composite hot-pressed at 560 °C (measured to be 2.646 g/cm^3) was very close to the theoretical density (2.653 g/cm^3), i.e. the relative density reaches 99.8%. This value is higher (~99.9%) for the composite hot-pressed at 620 °C.

The TEM specimens were taken at different positions of the composite discs to make sure that the microstructures observed are prevalent throughout the samples. Thin foil specimens for TEM observations were prepared by mechanical polishing from 500 μm to 30 μm, then dimpled by diamond paste to 10 μm, and finally thinned by ion-milling using Gatan PIPS 695 at approximately −100 °C. Microstructure characterizations and X-ray energy-dispersive spectroscopy (EDS) analysis were performed in a FEI Tecnai F30 G^2 TEM and the atomic-resolution HAADF-STEM imaging was carried out in a FEI Titan G^2 60-300 Cs-corrected TEM.

3. Results

Fig. 1a shows a HAADF image of a B_4C reinforcement in the composite hot-pressed at 560 °C. It remains the polygonal morphology as the as-received B_4C particles. The different contrasts in the B_4C particle originate from the inhomogeneous thickness along the electron beam direction. A high-magnification TEM image of the interface between a B_4C particle (left) and the alloy matrix (right) is displayed in Fig. 1b. The clean and sharp interface indicates that no chemical reaction occurred at this temperature.

In this composite, Cu presents in the form of precipitation particles with sizes of several tens nanometers, as marked by white arrows in Fig. 2a. The bright contrast of these precipitates in this image implies that they contain heavy atoms, since the contrast intensity in the HAADF mode is in proportion to $Z^{1.7\sim1.9}$, where Z is the atomic number [23]. Fig. 2b shows a typical precipitate particle whose diameter is measured to be near 100 nm. Most particles in the composite have smaller sizes. Electron diffraction analysis indicated that the precipitates were randomly oriented. The chemical composition analyzed by EDS demonstrated that the precipitates were composed of Al, Mg, Si and Cu (as shown in Fig. 2c). The chemical composition and selected area electron diffraction (SAED) pattern (Fig. 2d) can lead to the conclusion that these particles are Q phase which is the equilibrium precipitate in Al-Mg-Si-Cu alloys. The Q phase has a hexagonal structure with the lattice parameter of $a = 1.04$ nm and $c = 0.405$ nm. The structures of Q phase and several precursors have been extensively studied by previous studies [11].

As the pressing temperature increased to 620 °C, the interfacial reactions between B_4C reinforcements and the alloy matrix occurred. Fig. 3a shows a B_4C particle embedded in the composite. Compared with that in Fig. 1a, the B_4C/matrix interface exhibits a distinct morphology. A continuous layer of reaction products which consisted of a series of nanoparticles appeared at the interface. An individual nanoparticle is displayed in the TEM image shown in Fig. 3b. The SAED pattern inset in the figure indicates the particles are Al_3BC crystals (hexagonal structure, a = 0.349 nm, c = 1.154 nm).

We then carried out EDS elemental mapping on an Al_3BC particle (Fig. 4a). The mapping reveals that it is composed of Al, B, C, and a small amount of Si. It is interesting to note that the particle is enclosed by a thin layer of Cu. An atomic resolution HAADF-STEM image of the interface area is shown in Fig. 4b, where the Cu-rich atmosphere around the particle with brighter contrast is clear seen, in accordance with the EDS result. The thickness of the layer is measured to be about 0.7 nm.

Accompanied with Al_3BC particles, the B_4C/alloy reactions also resulted in the formation of a high density of nanoscaled precipitates in the alloy matrix. Meanwhile, the Q phase was rarely observed. Fig. 5a shows a low-magnification HAADF image of these lath-shaped precipitates with diameters of several tens of nanometers and lengths ranging from 100 nm to several micrometers. By EDS and diffraction analysis, they are identified to be MgB_2

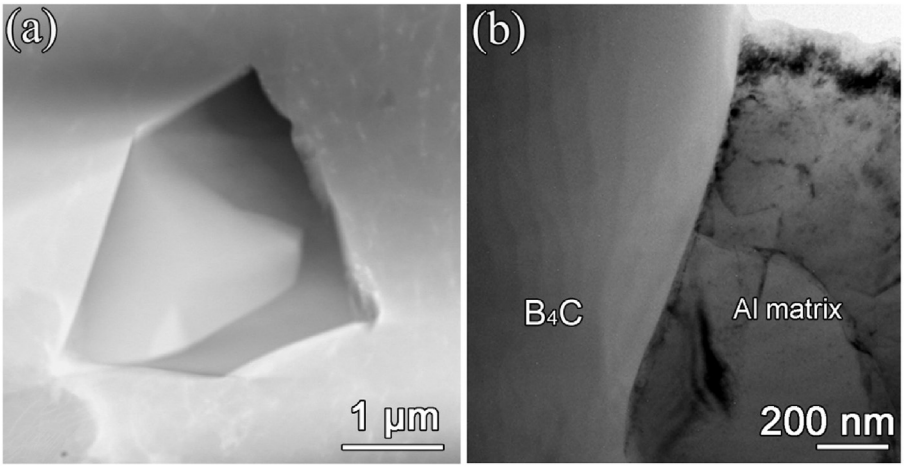

Fig. 1. Morphology of the B_4C reinforcement in the composite hot-pressed at 560 °C. (a) HAADF image of the B_4C particle embedded in Al matrix. It remains the polygonal shape as the as-received state. (b) TEM image of the B_4C/matrix interface showing no chemical reaction occurred here.

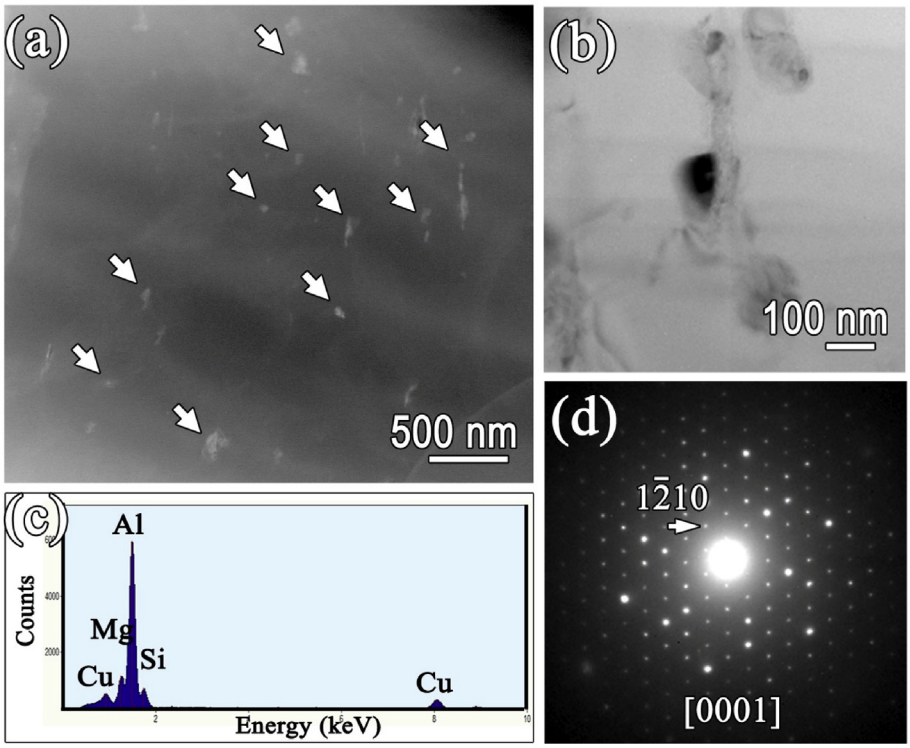

Fig. 2. Characterization of the Q phase which is the main precipitate in the composite fabricated at low temperature. (a) Low-magnification HAADF image showing the dispersive precipitates in the alloy matrix. (b) A typical Q phase with diameter of ~100 nm. (c) EDS analysis indicating the particle contains Al, Mg, Si and Cu. (d) Selected area electron diffraction (SAED) pattern of the particle in (b).

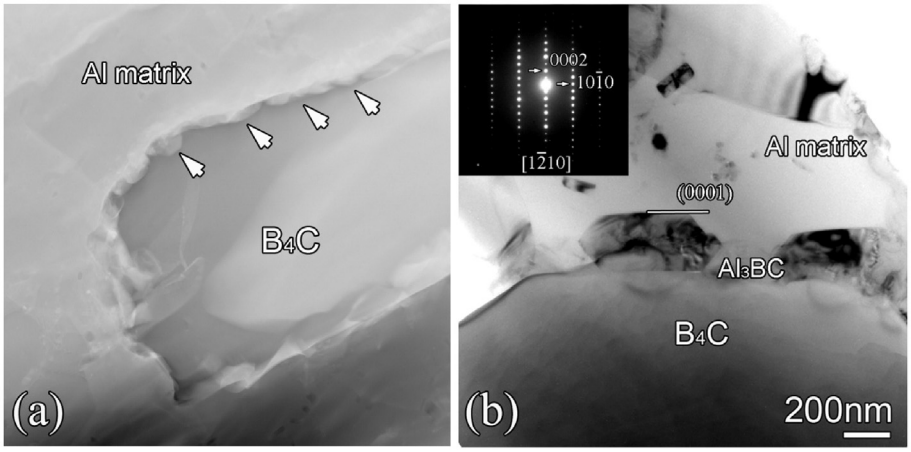

Fig. 3. B_4C particle in the composite hot-pressed at 620 °C. (a) Low-magnification HAADF image of the particle. The reaction products continuously distribute along the B_4C/matrix interface (as arrowed). (b) TEM image of the nanoparticles at the interface. The inset SAED pattern can be indexed as the $[1\bar{2}10]$ zone axis of Al_3BC phase.

crystals (hexagonal structure, a = 0.309 nm, c = 0.352 nm [24]). The randomly oriented MgB_2 precipitates in Fig. 5a indicate that there is no specific crystallographic orientation relationship between MgB_2 and the matrix. Fig. 5b and c display the TEM images as well as the corresponding SAED patterns of the crystal viewed along two vertical directions, i.e. $[\bar{2}110]$ and [0001]. The 3D information in the TEM images demonstrates that the MgB_2 crystal has prism morphology and the prismatic surfaces are $\{01\bar{1}0\}$ planes.

Cu concentration was also observed at MgB_2/matrix interfaces when we performed the EDS elemental mapping on the area framed in Fig. 6a. As illustrated in Fig. 6b (the left column is EDS maps of B, Mg and Cu, the right column is the intensity graphs digitally transformed from the EDS signals to enhance the intensity contrast), the MgB_2 prismatic surfaces are covered by a thin layer composed of Cu, while no obvious Cu signal is detected on the {0001} surface. The interfacial Cu enrichment was observed on all the MgB_2 precipitates, no matter what size they possess. Taking a careful inspection on the distributions of the three compositions, we could find that Cu-enriched layer also contained a small amount of magnesium but no boron. The result is reasonable since Cu and Mg can easily form intermetallic compounds because of the high affinity between them and Cu–B binary systems with high Cu content is unstable [25]. Fig. 6b is high-magnification HAADF image of the MgB_2/matrix interface where a double-atomic layer of Cu

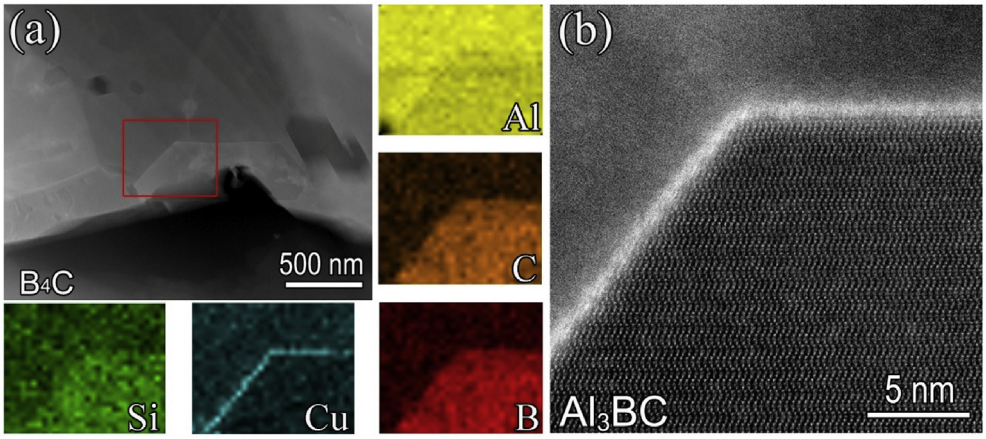

Fig. 4. Characterization of Cu segregation at the Al_3BC/matrix interface. (a) HAADF image and the EDS elemental mapping performed on the area marked by a rectangle. (b) High resolution HAADF image showing the Al_3BC particle is surrounded by a thin layer of Cu.

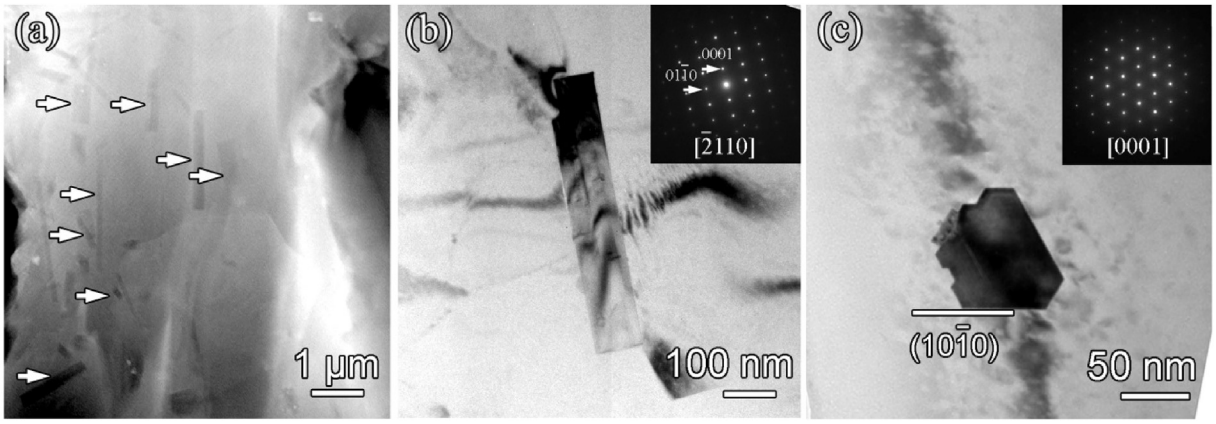

Fig. 5. MgB_2 nanorods generated by chemical reactions between B_4C and the alloy matrix. (a) Low-magnification HAADF image showing the dispersive MgB_2 nanorods in the alloy matrix. (b) and (c) TEM images and the corresponding SAED patterns of the MgB_2 precipitate viewed along its [$\bar{2}$110] zone axis and [0001] zone axis, respectively.

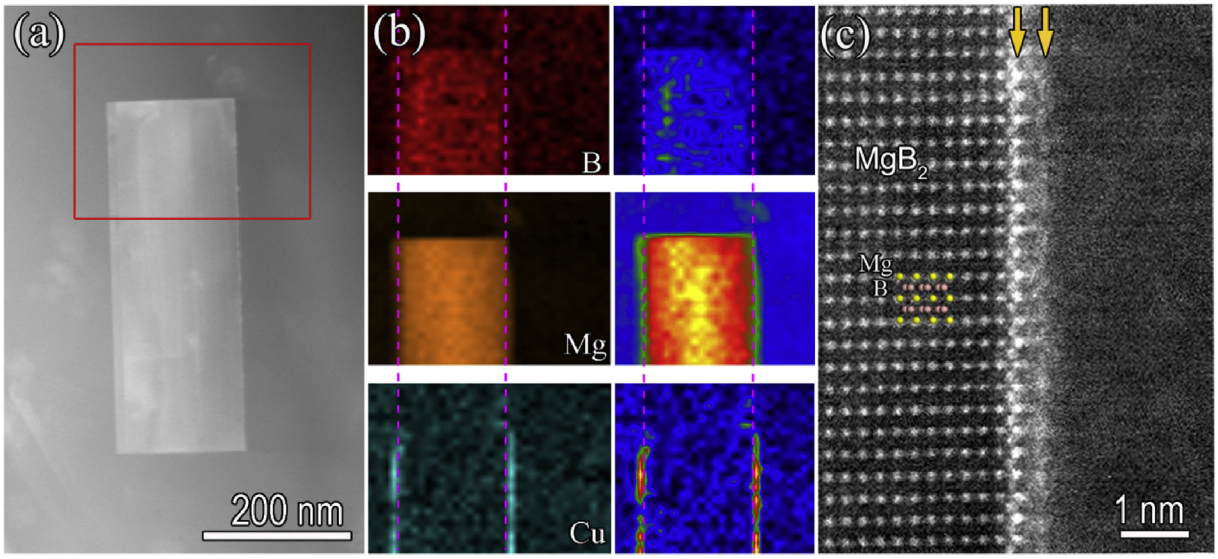

Fig. 6. Solute segregation at the MgB_2/matrix interface. (a) HAADF image of a B_4C/Al interface where the Al_3BC particles are clearly seen. (b) EDS chemical maps of B, Mg and Cu (the left column) and 2D intensity maps with enhancing contrast (the right column). It is seen that the interface is Cu-enriched but B-depleted, and the content of Mg in this layer is a little higher than in the matrix. (c) Segregated atoms form a double-atomic layered shell on the surface of MgB_2 precipitate.

atoms can be clear seen, as denoted by yellow arrows. In the layer, Cu and Mg atoms seem to regularly arrange and form a crystalline layer.

Meanwhile, several nanoparticles are found to decorate at the MgB_2/matrix interface. These particles with diameters of 1–3 nm are commonly seen at the interfaces. They are easily confused with the copper enriched layer. EDS mapping (Fig. 7a) indicates that it is not a copper compound but enriched of vanadium which is the impurity element in B_4C powder. Fig. 7b shows the atomic structure of a decorating nanoparticle which keeps an epitaxial relation with the $(10\bar{1}0)$ plane of the MgB_2 crystal. Through the Fast Fourier Transform (FFT) pattern (as inset), we can identify the particle as VB_2 which has a similar structure with MgB_2.

4. Discussion

In the present work, we characterized the precipitates as well as the distributions of alloying element Cu in B_4C-reinforced 6061 Al composites fabricated below and above the temperature at which B_4C particles reacted with the alloy matrix. In the composites hot-pressed below that temperature, Cu presented in the form of nano-sized Q phase. Since no B_4C/alloy reaction occurred in the composite, the precipitation and the role of Cu played should be analogous to that in Al-Mg-Si-Cu alloys which have been well documented in several studies [9,10,14]. The discussion will therefore focus on the effect of Cu on the interfacial reactions.

The characterization on the composite fabricated above 620 °C indicates the interfacial reactions gave rise to a tremendous change of the precipitates. Specifically, the boron-contained reaction products, such as Al_3BC and MgB_2 replaced the Q phase. The process should be ascribed to the chemical reactions facilitated by the appearance of molten alloy. The reactions can be written as:

$$3Al + B_4C \rightarrow Al_3BC + 3B \quad (1)$$

$$2B + Mg \rightarrow MgB_2 \quad (2)$$

Reaction (1) mainly occurred at the interphase boundaries where the B_4C and Al melt directly contact. Al_3BC, as a reaction product in B_4C reinforced AMCs were observed by most researchers [17,20,26]. Besides Al_3BC, free boron was also generated by this reaction and then diffused into the alloy matrix. The large electronegativity difference between Mg and B made the two elements easily combine and produce MgB_2 (reaction (2)). This reaction consumed the solute Mg and suppressed the formation of Q phase in alloy matrix as a result. When the alloying Mg was exhausted, excess boron might react with other elements, for example, the impurity vanadium.

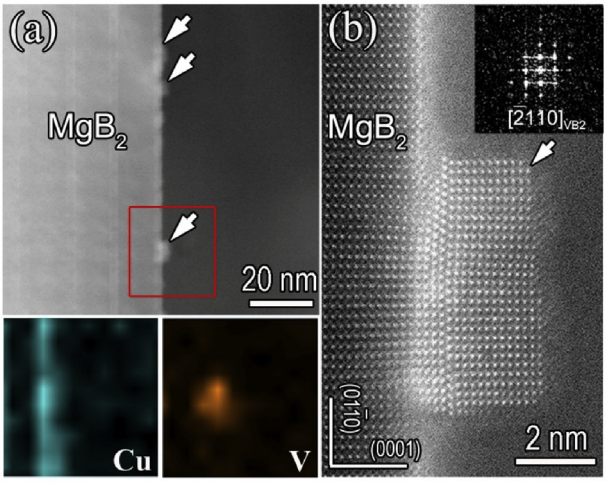

Fig. 7. VB_2 nanoparticles decorating at the MgB_2/matrix interfaces (a) HAADF image and elemental mappings derived from the EDS signals of Cu and V. (b) High resolution HAADF image showing the VB_2 nanocrystal epitaxially grows on the surface of MgB_2.

Instead of forming new precipitates, the solute element Cu segregated at the interphase boundaries of precipitates Al_3BC or MgB_2. Interfacial segregation of solute atoms has been observed in several aluminum alloys and is receiving increasing interest in these years. For example, Cu segregation at Q/Al interfaces in a Al-Mg-Si-Cu alloy was reported in Fiawoo et al.'s recent work [16]. Some other results include Mg segregation at Al_3Sc/Al interfaces in Al-Mg-Sc alloys [27], Si segregation at θ'/Al interfaces in Al-Si-Cu alloys [28], and Mg-Ag co-segregating at Ω/Al interfaces in Al-Cu-Mg-Ag alloys [29], *etc.* Similar solute segregation at heterophase interface has also been detected in magnesium alloys [30,31]. Although some explanations of the interface segregation have been proposed, the most commonly accepted one is that the solute segregation can reduce the interfacial energy [8,28]. The reduction of interfacial energy would lead to the enhancing nucleation rate and the coarsening-resistance of the precipitates. In the present composite, it is believed that the Cu should have the same effect, which is in agreement with the experimentally observed high density of nano-sized precipitates (as shown in Figs. 3a and 5a).

The interfacial reaction products, including their species, shapes and sizes, are believed to significantly influence the loading transfer between reinforcements and matrix, and consequently the mechanical property of the composite [32]. In the future work, it is worthwhile studying the microalloying effect on the mechanical properties of AMCs.

5. Conclusion

In the present work, the precipitates in B_4C/6061 Al composites fabricated at different temperatures, especially the distribution of minor alloying element Cu were investigated. The precipitates in the composites are highly influenced by the interfacial reactions between B_4C reinforcements and the Al matrix: the fine Al_3BC and MgB_2 particles replaced the Q phase which was the main precipitate in the composite without interfacial reactions. Cu segregation at the Al_3BC/matrix and MgB_2/matrix interfaces leading to decrease in interfacial free energy should be responsible for the high nucleation rate of the precipitates.

Acknowledgements

This work is supported by the National Natural Science Foundation of China (U1508216, 51501195 and 51671191) and the Innovation Fund of IMR (2017-PY10). Mr. B. Wu and L.X. Yang of this laboratory are acknowledged for their technical support on TEM experiments.

References

[1] X.-G. Chen, Application of Al–B_4C metal matrix composites in the nuclear industry for neutron absorber materials, in: N. Gupta, W.H. Hunt (Eds.), Solidification Processing of Metal Matrix Composites, TMS, USA, 2006, pp. 343–350.
[2] P. Zhang, Y. Li, W. Wang, Z. Gao, B. Wang, The design, fabrication and properties of B4C/Al neutron absorbers, J. Nucl. Mater. 437 (2013) 350–358.
[3] X.-G. Chen, L. St-Georges, M. Roux, Mechanical behavior of high boron content Al-B_4C metal matrix composites at elevated temperatures, Mater. Sci. Forum 706–709 (2012) 631–637.
[4] X. Yue, J. Wang, Y. Li, H. Ru, Properties of B_4C/Al–B_4C composite with a two-layer structure, Mater. Res. Bull. 48 (2013) 1720–1724.
[5] H.S. Chen, W.X. Wang, Y.L. Li, P. Zhang, H.H. Nie, Q.C. Wu, The design, microstructure and tensile properties of B_4C particulate reinforced 6061Al

neutron absorber composites, J. Alloys Compd. 632 (2015) 23–29.
[6] K. Lindquist, Handbook on Neutron Absorber Materials for Spent Nuclear Fuel Transportation and Storage Applications, 2009 ed., EPRI, Palo Alto, CA, 2009, 7.1-7.68.
[7] S.P. Ringer, K. Hono, Microstructural evolution and age hardening in aluminium alloys: atom probe field-ion microscopy and transmission electron microscopy studies, Mater. Charact. 44 (2000) 101–131.
[8] I.J. Polmear, D. StJohn, J.F. Nie, M. Qian, Light Alloys, fifth ed., Elsevier, 2017.
[9] R.J. Livak, The effects of copper and chromium on the aging response of dilute Al-Mg-Si alloys, Metall. Trans. A 13 (1982) 1318–1321.
[10] J. Man, L. Jing, S.G. Jie, The effects of Cu addition on the microstructure and thermal stability of an Al–Mg–Si alloy, J. Alloys Compd. 437 (2007) 46–50.
[11] D.J. Chakrabarti, D.E. Laughlin, Phase relations and precipitation in Al–Mg–Si alloys with Cu additions, Prog. Mater. Sci. 49 (2004) 389–410.
[12] Y. Weng, Z. Jia, L. Ding, Y. Pan, Y. Liu, Q. Liu, Effect of Ag and Cu additions on natural aging and precipitation hardening behavior in Al-Mg-Si alloys, J. Alloys Compd. 695 (2017) 2444–2452.
[13] H.S. Hasting, J.C. Walmsley, A.T.J. Van Helvoort, C.D. Marioara, S.J. Andersen, R. Holmestad, Z-contrast imaging of the arrangement of Cu in precipitates in 6XXX-series aluminium alloys, Phil. Mag. Lett. 86 (2006) 589–597.
[14] C.D. Marioara, S.J. Andersen, T.N. Stene, H. Hasting, J. Walmsley, A.T.J. Van Helvoort, R. Holmestad, The effect of Cu on precipitation in Al–Mg–Si alloys, Phil. Mag. 87 (2007) 3385–3413.
[15] T. Saito, C.D. Marioara, S.J. Andersen, W. Lefebvre, R. Holmestad, Aberration-corrected HAADF-STEM investigations of precipitate structures in Al–Mg–Si alloys with low Cu additions, Phil. Mag. 94 (2013) 520–531.
[16] M. Fiawoo, X. Gao, L. Bourgeois, N. Parson, X.Q. Zhang, M. Couper, J.F. Nie, Formation of multiple orientation relationships of Q precipitates in Al-Mg-Si-Cu alloys, Scr. Mater. 88 (2014) 53–56.
[17] Z. Luo, Y. Song, S. Zhang, D.J. Miller, Interfacial microstructure in a B_4C/Al composite fabricated by pressureless infiltration, Metall. Mater. Trans. A 43 (2011) 281–293.
[18] J. Lai, Z. Zhang, X.-G. Chen, Effect of Sc, Zr, and Ti on the interfacial reactions of the B_4C/Al system, J. Mater. Sci. 46 (2010) 451–459.
[19] Y.Z. Li, Q.Z. Wang, W.G. Wang, B.L. Xiao, Z.Y. Ma, Effect of interfacial reaction on age-hardening ability of B_4C/6061Al composites, Mater. Sci. Eng. A 620 (2015) 445–453.
[20] Y.Z. Li, Q.Z. Wang, W.G. Wang, B.L. Xiao, Z.Y. Ma, Interfacial reaction mechanism between matrix and reinforcement in B_4C/6061Al composites, Mater. Chem. Phys. 154 (2015) 107–117.
[21] J.M. Rosalie, L. Bourgeois, Silver segregation to θ′ (Al_2Cu)–Al interfaces in Al–Cu–Ag alloys, Acta Mater. 60 (2012) 6033–6041.
[22] X.H. Shao, Z.Z. Peng, Q.Q. Jin, X.L. Ma, Atomic-scale segregations at the deformation-induced symmetrical boundary in an Mg-Zn-Y alloy, Acta Mater. 118 (2016) 177–186.
[23] S.J. Pennycook, Structure determination through Z-contrast microscopy, Adv. Imag. Electron Phys. 123 (2002) 173–206.
[24] J. Nagamatsu, N. Nakagawa, T. Muranaka, Y. Zenitani, J. Akimitsu, Superconductivity at 39 K in magnesium diboride, Nature 410 (2001) 63–64.
[25] A.C. Tampieri, G. Celotti, S. Sprio, D. Rinaldi, G. Barucca, R. Caciuffo, Effects of copper doping in MgB_2 superconductor, Solid State Comm. 121 (2002) 497–500.
[26] Z. Zhang, X.-G. Chen, A. Charette, Fluidity and microstructure of an Al–10% B_4C composite, J. Mater. Sci. 44 (2009) 492–501.
[27] E.A. Marquis, D.N. Seidman, M. Asta, C. Woodward, V. Ozolins, Mg segregation at Al/Al_3Sc heterophase interfaces on an atomic scale: experiments and computations, Phys. Rev. Lett. 91 (2003) 036101.
[28] A. Biswas, D.J. Siegel, D.N. Seidman, Simultaneous segregation at coherent and semicoherent heterophase interfaces, Phys. Rev. Lett. 105 (2010) 076102.
[29] S.J. Kang, Y.-W. Kim, M. Kim, J.-M. Zuo, Determination of interfacial atomic structure, misfits and energetics of Ω phase in Al–Cu–Mg–Ag alloy, Acta Mater. 81 (2014) 501–511.
[30] C. Liu, H. Chen, J.F. Nie, Interphase boundary segregation of Zn in Mg-Sn-Zn alloys, Scr. Mater. 123 (2016) 5–8.
[31] D. Rossouw, B. Langelier, A. Scullion, M. Danaie, G.A. Botton, Multivariate-aided mapping of rare-earth partitioning in a wrought magnesium alloy, Scr. Mater. 124 (2016) 174–178.
[32] M.M. Kouzeli, C.S. Marchi, A. Mortensen, Effect of reaction on the tensile behavior of infiltrated boron carbide aluminium composites, Mater. Sci. Eng. A 337 (2002) 264–273.